

The Effects of X-Ray and UV Background Radiation on the Low-Mass Slope of the Galaxy Mass Function

D.C. Hambrick^{1*}, J.P. Ostriker¹, P.H. Johansson², and T. Naab²

¹*Princeton University Observatory, Princeton, NJ 08544*

²*University Observatory Munich, Scheinerstr. 1, 81679 Munich, Germany*

1 October 2010

ABSTRACT

Even though the dark-matter power spectrum in the absence of biasing predicts a number density of halos $n(M) \propto M^{-2}$ (i.e. a Schechter α value of -2) at the low-mass end ($M < 10^{10} M_{\odot}$), hydrodynamic simulations have typically produced values for stellar systems in good agreement with the observed value $\alpha \simeq -1$. We explain this with a simple physical argument and show that an efficient external gas-heating mechanism (such as the UV background included in all hydro codes) will produce a critical halo mass below which halos cannot retain their gas and form stars. We test this conclusion with GADGET-2-based simulations using various UV backgrounds, and for the first time we also investigate the effect of an X-ray background. We show that at the present epoch α is depends primarily on the mean gas temperature at the star-formation epoch for low-mass systems ($z \lesssim 3$): with no background we find $\alpha \simeq -1.5$, with UV only $\alpha \simeq -1.0$, and with UV and X-rays $\alpha \simeq -0.75$. We find the critical final halo mass for star formation to be $\sim 4 \times 10^8 M_{\odot}$ with a UV background and $\sim 7 \times 10^8 M_{\odot}$ with UV and X-rays.

Key words: galaxies: dwarf — galaxies: formation — methods: numerical

1 INTRODUCTION

The mass spectrum of dark-matter (DM) halos collapsing from an initial gaussian-perturbed density field has long been an object of study; the formalism most widely used today is that of Press & Schechter (1974), who derived a number density of the form

$$n(M)dM = M^{-2} \bar{\rho} \sqrt{2/\pi} \frac{\delta_c}{\sigma} \frac{d \ln \sigma^{-1}}{d \ln M} e^{-\delta_c^2/2\sigma^2} dM \quad (1)$$

where $n(M)dM$ is the number of halos in the mass range M to $M + dM$, $\bar{\rho}$ is the mean mass density, δ_c is the critical (linear) density for collapse, and σ is the rms perturbation. If we consider small scales, where σ is both $\gg \delta_c$ and approximately independent of mass, then the Press-Schechter form reduces to

$$n(M)dM \propto M^{-2} dM \quad (2)$$

(Chiu, Gnedin & Ostriker 2001).

The luminosity function of galaxies is commonly parametrized in the Schechter form (Schechter 1976),

$$n(L)dL \propto (L/L_*)^{\alpha} e^{-L/L_*} dL; \quad (3)$$

i.e., a power-law of slope α at the low-luminosity end with an

exponential cutoff at a characteristic luminosity L_* . If star formation traced the underlying dark matter distribution exactly (i.e. a constant mass-to-light ratio), we would expect to observe $\alpha \simeq -2$ at the faint end. However, galaxy surveys such as the SDSS have consistently shown a different slope, in the range of $-1.2 \lesssim \alpha \lesssim -0.9$ (see Blanton et al. 2001, Table 2 of Alimi & Courty 2005, and Pérez-González et al. 2008). The extent to which galaxies or dark-matter halos fail to follow the clustering distribution of linear perturbation theory is known generally as “bias”, and has been an active area of phenomenological and theoretical research (see, e.g., the introduction to Benson et al. 2000 and §6 of Cooray & Sheth 2002 for an overview): most relevant here is the relative bias between galaxies and DM halos, i.e. the extent to which galaxies fail to follow the underlying DM. At the low-mass end, the discrepancy has come to be called the “missing satellites problem” (Klypin et al. 1999), since naïve Press-Schechter theory predicts ~ 300 satellite galaxies for the Local Group, while only ~ 40 are observed (Simon & Geha 2007)—although this number continues to increase as data from e.g. SDSS are analyzed.

One might expect that this relative bias would be a concern for those performing galaxy simulations, and indeed DM-only simulations which assign galaxies to DM halos after the fact (e.g., the Millennium Run of Springel et al. 2005) do use an ad-hoc prescription to reduce the baryonic mass in

* E-mail: dclayh@astro.princeton.edu

small halos, or overpredict small halos (De Lucia & Blaizot 2007), although agreement is improving as semianalytic models improve in sophistication (Guo et al. 2010b). However, hydrodynamic simulations seem to require no such prescription: they most often report a faint-end mass spectrum slope in the vicinity of $-0.9 - -1.2$ (Chiu, Gnedin & Ostriker 2001; Nagamine et al. 2005; Alimi & Courty 2005). While there are some exceptions (Oppenheimer et al. 2009 report $\alpha = -1.45$ for their best-fit model; Crain et al. 2009 find $\alpha = -1.96$), it would appear this is a result which is difficult to get wrong.

Dekel & Silk (1986) were the first to propose a mechanism of gas being heated (by local supernovae) and driven out of low-mass halos. Efstathiou (1992) introduced the idea of the ionizing background radiation being the relevant mechanism, and Quinn, Katz, & Efstathiou (1996) used a smooth particle hydrodynamic (SPH) simulation to show that a photoionizing background does strongly inhibit the cooling and infall of gas into halos of virial mass below $4 \times 10^9 M_\odot$. Thoul & Weinberg (1996) did the same with a 1D Lagrangian code. Navarro & Steinmetz (1997) showed that the UV background reduced the cooled gas accreted to disk galaxies by half, with late-accreting gas preferentially affected. Gnedin (2000) used simulations of reionization to determine that the mass scale at which gas is stripped by photoionization from the background radiation corresponds to the “filtering” length scale, the scale at which baryonic matter is smoothed compared to the underlying dark matter in linear perturbation theory; however Okamoto et al. (2008) using GADGET-2 found a somewhat smaller critical mass of $10^{10} M_\odot$ (similar values were obtained by Hoefl et al. 2006 and Crain et al. 2007) and, significantly, reported that their SPH result was well approximated by a simple prescription comparing the gas temperature to the virial temperature of the halo. Benson et al. (2002) and Somerville (2002) made semianalytic calculations of galaxy evolution and likewise found that galaxies fainter than L_* have their star formation suppressed or “squashed” by a photoionizing background. Meanwhile, the role of supernova feedback in driving gas from small halos and thereby suppressing star formation has continued to be studied (Yepes et al. 1997; Kay et al. 2002; Scannapieco et al. 2008). Petkova & Springel (2010) have even performed a simulation showing that the UV output of local stars can affect the SFR. However, while these processes are certainly present and important, our focus here is on the ionizing background, which we will show to be both necessary and sufficient to reproduce the observed Schechter α .

It should be noted that despite the terminology of “critical” or “cutoff” masses, a sharp cutoff in galaxy masses is not consistent with the observations: there are low-mass (dwarf) galaxies, merely fewer than expected. Several mechanisms have been proposed to explain this. Shaviv & Dekel (2003) proposed that some intermediate-mass halos ($v_{\text{circ}} \sim 25 - 35$ km/s, or $M \sim 10^{10} M_\odot$) have star formation at early times, then lose their remaining gas at the time of reionization and become “red and dead” dwarfs at the present. Kravtsov et al. (2004) suggested that present dwarf satellites such as those around the Milky Way were originally larger but were reduced to their present size by tidal stripping. Such mechanisms may be needed to explain the very low luminosity ($\gtrsim 10^3 L_\odot$) Milky Way satellites discovered

in recent years (Willman et al. 2005; Belokurov et al. 2006, 2007).

Two recent studies are of particular interest. Sawala et al. (2010) studied the evolution of dwarf galaxies in isolation and found that both feedback and a UV background are necessary to reproduce the observed properties of the Local Group dwarf spheroidals. In particular, they saw that the UV background efficiently suppresses star formation after the epoch of reionization for systems below $10^9 M_\odot$. Similarly, Okamoto & Frenk (2009) simulate a Milky Way-like galaxy and its satellites and find a threshold circular speed of 12 km/s ($\sim 8 \times 10^8 M_\odot$) for halos which can form stars.

We also note that even though it has been known at least since Madau & Efstathiou (1999) that including the X-ray background has a substantial effect on the temperature of the IGM (and hence, as we will see, on star formation), few simulations have incorporated this component. Ricotti et al. (2008) studied its effect on dwarf galaxies and found a critical baryon retention mass, but only looked at $z > 8$. We remedy this deficit by including an X-ray background in some of our simulations to study its effect on small galaxies from moderate redshift to the present.

In a previous paper (Hambrick et al. 2009, hereafter Paper I), we explored the effect of the ionizing background on the stellar and gas properties of large elliptical galaxies. Here, we use a similar set of UV and X-ray backgrounds to examine their effect on the low end of the galaxy mass spectrum, namely the satellites of those ellipticals. Section 2 presents a simple physical argument for why any efficient gas-heating mechanism will yield a flattening of the low-mass slope. Section 3 presents the details of the simulations we performed to test this argument; section 4 gives the results of the same. Section 5 is discussion and conclusions.

2 PHYSICAL ARGUMENT

Our argument, which dates back to Rees (1986) and Efstathiou (1992), compares the escape velocity of gas in a virialized halo to the sound speed of that gas. The escape velocity for a halo of mass M and radius r is given by

$$v_{\text{esc}} = \sqrt{\frac{2GM}{r}}. \quad (4)$$

We relate M and r by fixing the density at the standard “virialized” value,

$$\rho = 200\bar{\rho}$$

where $\bar{\rho}$ is the mean density of the universe at a given epoch (we calculate the result for $z = 0$, and assume $\Omega_M = 0.3$, as in our simulations). Then the escape velocity becomes

$$\begin{aligned} v_{\text{esc}} &= \sqrt{2G \left(\frac{800\pi}{3} \bar{\rho} M^2 \right)^{1/3}} \\ &= 36.0 \left(\frac{M}{10^{10} M_\odot} \right)^{1/3} \text{ km/s}. \end{aligned} \quad (5)$$

The sound speed, meanwhile, is given for a gas of temperature T and mean particle mass m by

$$\begin{aligned}
 v_c &= \sqrt{\frac{\gamma k T}{m}} \\
 &= 21.7 \left(\frac{T}{10^5 \text{K}} \right)^{1/2} \text{ km/s},
 \end{aligned}
 \tag{6}$$

where we assume the adiabatic index $\gamma = 5/3$ for non-relativistic gas, and for m we assume primordial abundances of H and He. By equating these speeds, we have a formula for a critical mass:

$$M_{\text{crit}} = 2.19 \times 10^9 \left(\frac{T}{10^5 \text{K}} \right)^{3/2} M_{\odot}
 \tag{7}$$

At a given gas temperature, halos below this critical mass will have gas thermal speeds greater than their escape velocities. Hence they will not be able to hold on to their gas, and therefore be unable to form stars. For a temperature of 2×10^4 K, corresponding to the peak of the H cooling curve, $M_{\text{crit}} = 2 \times 10^8 M_{\odot}$. Therefore we expect halos with less than this total mass to have very little star formation, and at late times, very little baryonic mass of any kind, assuming there is a mechanism to heat the gas to 2×10^4 K by the epoch where star formation in these halos would be significant. Heating above this temperature will further increase the cutoff mass. Moreover, since larger systems are formed by the hierarchical assembly of smaller ones, we expect this baryon deficit to creep to larger-mass halos as time passes, effectively increasing the critical mass at the present by some factor $f \gtrsim 1$.

3 SIMULATIONS

To verify the physical argument presented above, we analyze several high-resolution simulations that are performed with various ionizing (UV and X-ray) backgrounds. These simulations were performed with a slightly updated version of the GADGET-2-based code used in Paper I; refer to that work for additional details. In brief, the code is based on GADGET-2, and the halos are selected from a $(50 \text{ Mpc})^3$ box with cosmological (Λ CDM) initial conditions, and resimulated in a $(1 \text{ Mpc})^3$ box centered on each halo, with the central $(0.5 \text{ Mpc})^3$ using high-resolution DM and gas/star particles (for more details see Naab et al. 2007; Johansson, Naab & Ostriker 2009). Since we specifically select high-density regions containing massive galaxies, our results are not necessarily applicable to other environments. To ameliorate the effects of cosmic variance, we choose seven galaxies (that is, seven initial-conditions (IC) boxes), with final virial masses in the range $1 - 2 \times 10^{12} M_{\odot}$. The simulations do not include optical depth effects, in particular the self-shielding of dense star-forming regions from the UV background. They do (differently from Paper I) include feedback from supernovae though not AGN, following the two-phase Springel & Hernquist (2003) model, and a simple prescription for metal-line cooling using cooling rates calculated by Cloudy (v07.02, last described in Ferland et al. 1998), which presumes photoionization and collisional equilibrium for the gas and metal atoms, and assumes 0.1 solar metallicity. Star formation is performed at a fixed density threshold calculated by the code such that $\sim 90\%$ of the gas above the threshold will be in cold phase: this threshold is

$\rho_{\text{crit}} = 1.6 \times 10^{-25} \text{ g cm}^{-3}$ or $n_{\text{H,crit}} = 0.07 \text{ cm}^{-3}$. Star particles have half the mass of original gas particles; thus each gas particle can ultimately turn into two star particles. As in Paper I, all simulations were performed with initially 100^3 each of SPH (i.e. baryon) particles and DM particles, with a gravitational softening length of 0.25 kpc for the gas and star particles and twice that for the dark matter particles. Gas and star particles have masses in the range $4 - 7 \times 10^5 M_{\odot}$, depending on the size of the box; the assumed cosmology is $(\Omega_M, \Omega_{\Lambda}, \Omega_b/\Omega_M, \sigma_8, h) = (0.3, 0.7, 0.2, 0.86, 0.65)$.

We run these simulations using a variety of ionizing backgrounds: the same set which was used in Paper I, with two additions. The first, which we call No UV, has as the name suggests no ionizing radiation at all. The next three backgrounds are Old UV, an updated version of Haardt & Madau (1996); New UV, which has the same spectrum as Old UV but an intensity (as measured by e.g. the H photoionization rate) which declines as $(1+z)^{-1}$ above the peak at $z \simeq 2.2$; and FG UV, the background constructed in Faucher-Giguère et al. (2009). The final two backgrounds add an X-ray component, which has a spectrum taken from Sazonov, Ostriker, & Sunyaev (2004) and a normalization from Gilli et al. (2007). The New UV+X model takes the New UV model and adds this X-ray component with the same redshift dependence, while FG UV+X adds this component to the FG UV background but with the redshift dependence of Old UV (i.e. Haardt & Madau 1996) to more closely replicate the quasar background that the X-ray component is meant to model. The quasar background peaks at $z \sim 2$ and becomes negligible for $z \gtrsim 3$ (Hopkins, Richards & Hernquist 2007).

4 SIMULATION RESULTS

4.1 Results at $z = 0$

Having performed the simulations, we identify virialized systems in both the star and total (stars plus gas plus DM) particle populations using AHF, the Amiga Halo Finder (Knollmann & Knebe 2009). AHF uses a density grid-tree method followed by the removal of unbound particles to find halos and subhalos, and returns the virial mass of each. The virial mass is defined as the total mass of all (relevant) particles inside the virial radius, which in turn is defined as the radius where the calculated density profile exceeds a threshold multiple of the critical density determined by cosmology and redshift (~ 200); for subhalos the virial radius is instead the largest radius of any particle which is gravitationally bound to the halo. See the AHF documentation for details.

Figure 1 shows the mass distribution of stellar systems (identified using star particles only). AHF can identify systems as small as $1.5 \times 10^7 M_{\odot}$, or about 40 star particles, but we adopt $10^8 M_{\odot}$ as a lower mass limit to ensure completeness. The mean number of systems (averaged over the seven ICs) in the lowest mass decade ($10^8 - 10^9 M_{\odot}$) declines from 131 with No UV to ~ 43 with the three UV models and ~ 20 for the two UV plus X-ray cases, differences of 36σ and 14σ respectively, while the number in the two highest mass bins ($> 10^{10} M_{\odot}$) remains nearly constant. As an aside, we expect these highest-mass bins will be high compared to the global spectrum because we specifically select

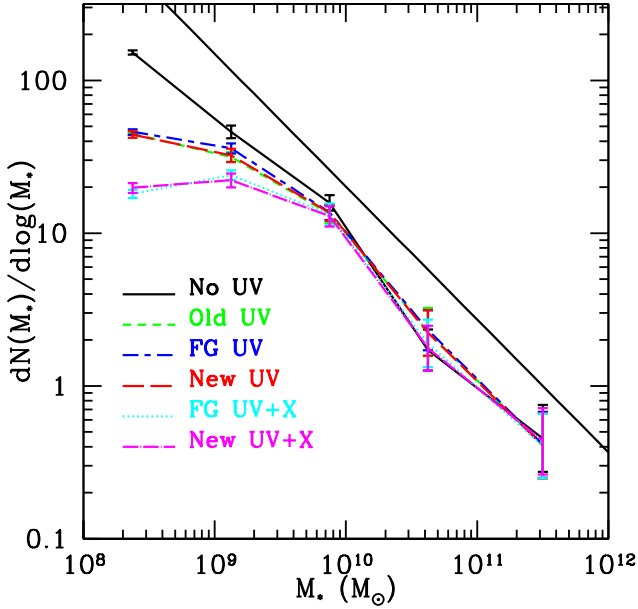


Figure 1. The average number of stellar systems (galaxies) per decade in stellar mass identified by AHF with mass in given range, at $z = 0$. The error bars represent 1σ statistical errors among the 7 initial conditions. Also included is an M^{-2} power law for comparison. The number of $< 10^9 M_\odot$ galaxies decreases markedly as one adds first UV and then X-ray radiation.

boxes which contain a massive galaxy; furthermore, systems of this virial mass ($M_{\text{Halo}} \approx 2 \times 10^{12} M_\odot$) have stellar masses which are very vulnerable to suppression by AGN feedback (e.g. McCarthy et al. 2010), not included here.

We also see that the UV-only models (Old UV, FG UV and New UV) are essentially identical to each other in mass spectrum. The two models with X-rays (New UV+X and FG UV+X) are also identical to each other, though of course quite different from the models without X-rays. This suggests that the details of the ionizing background above $z = 3$, including the epoch of reionization, are relatively unimportant in determining the mass spectrum.

Using the Bayesian inference method of Kelly, Fan, & Vestergaard (2008), we estimate the Schechter parameters α and M_* ; the results for α are presented in Table 1. This method has the advantage of not requiring any binning of the data. Values for M_* were roughly constant for the various background models in the range $10^{9.5-10} M_\odot$; also note that we use stellar mass as a proxy for luminosity without considering, e.g., age. Consistent with the appearance of Figure 1, α increases dramatically from -1.5 for the no-background case to roughly -1 for the UV-only models and -0.75 for the models with X-rays. Thus we see that the addition of a simple UV ionizing background was the only change necessary (with feedback; see below) to move the low end of the stellar mass spectrum into consistency with observations, while an additional X-ray background (which most simulations historically have not used) seems to make the slope *too* flat.

To directly compare these results with the mechanism presented in §2, we estimate fM_{crit} (the effective star-formation cutoff mass) by the following method. We take

Table 1. Schechter α values and maximum “barren” halo masses with various backgrounds.

Name	α	$\log fM_{\text{crit}}$	ϵ_*
No UV	-1.52 ± 0.06	8.19 ± 0.06	0.47 ± 0.02
Old UV	-1.01 ± 0.04	8.55 ± 0.08	0.37 ± 0.02
FG UV	-1.03 ± 0.06	8.50 ± 0.08	0.37 ± 0.02
New UV	-1.08 ± 0.05	8.63 ± 0.05	0.37 ± 0.02
FG UV+X	-0.73 ± 0.04	8.95 ± 0.07	0.32 ± 0.02
New UV+X	-0.78 ± 0.08	8.78 ± 0.04	0.32 ± 0.02
No UV-F	-1.64 ± 0.07	8.06 ± 0.06	0.48 ± 0.04
FG UV-F	-1.29 ± 0.06	8.22 ± 0.07	0.38 ± 0.04
FG UV+X-F	-1.16 ± 0.11	8.22 ± 0.09	0.33 ± 0.04

The Schechter- α values for the star particles, maximum “barren” halo masses, and overall baryon-conversion efficiency with various backgrounds. Adding UV and X-ray heating steadily increases α : models with UV only are consistent with observations. Similarly, the critical mass for baryon retention increases, and the baryon-conversion efficiency decreases, when the UV background and X-rays are added. The “-F” rows represent simulations with no SN feedback; see text for details.

the mass spectrum of halos identified by AHF from the total population of particles (stars, gas and DM), and find for each the total stellar mass in the halo. Then starting at the low-mass end of the spectrum we consider an 11-point moving average of the ratio of total stellar mass (M_*) to total overall virial mass (M_{Halo}) among the halos. (The number 11 was chosen to balance between mass resolution and the inherent scatter in stellar mass to total mass ratio among small halos, but even using a 41-point average does not significantly change the results.) We move upward through the mass spectrum until this ratio exceeds some fixed value, which we choose to be half of the global average (~ 0.16), which is the same definition as Gnedin (2000) and Okamoto et al. (2008). The particular choice of critical mass is not very important, as the baryon-conversion efficiency is a steep function of halo mass around the critical point (see Figure 2 of Okamoto et al. 2008)—even if we choose a threshold of one-tenth the global average, fM_{crit} falls by only ~ 0.2 dex. Thus fM_{crit} represents the largest total mass at which systems have severely restricted star formation. Mathematically:

$$fM_{\text{crit}} = M_{\text{Halo}}(N) \ni \frac{1}{2} \frac{\sum_i M_*(i)}{\sum_i M_{\text{Halo}}(i)} = \frac{\sum_{i=N-5}^{N+5} M_*(i)}{\sum_{i=N-5}^{N+5} M_{\text{Halo}}(i)} \quad (8)$$

The results are presented in the third column of Table 1. We find the critical mass in the No UV case is $1.5 \times 10^8 M_\odot$, but when a UV background is added this increases by a factor of more than 2 to $\sim 3.6 \times 10^8 M_\odot$, and with X-rays by another factor of 2 to $\sim 7.3 \times 10^8 M_\odot$, in good agreement with Okamoto & Frenk (2009), who also looked at satellite galaxies. They used a background with UV but not X-rays, but they did include supernova winds, which should act in a similar way as X-rays to blow out gas from small halos; thus we would expect our UV+X critical mass to be the most sim-

ilar to theirs, which is what we find. Okamoto et al. (2008), meanwhile, report a significantly higher value of $\sim 10^{10} M_{\odot}$ using only isolated halos; see the discussion in the next paragraph. We find (see §4.2) that No UV has a gas temperature at the star-forming epoch of 2×10^4 K, so comparing that cutoff mass to the value of $2 \times 10^8 M_{\odot}$ derived in §2, we find that the dimensionless hierarchical-structure correction factor $f \approx 0.75$, actually less than unity. This seems to support the idea of Kravtsov et al. (2004) that small satellites at late times were originally larger, and indicates that systems above the critical mass are able to accrete sufficient gas to overcome the deficit of accreted stars.

Finally, we revisit the finding in Paper I that overall star formation is suppressed with the ionizing background. To compare across the various initial conditions, we calculate the baryon-conversion efficiency, ϵ_{*} , defined as

$$\epsilon_{*} \equiv \frac{M_{*}}{M_b}$$

where M_{*} and M_b are the total stellar and baryonic (gas plus stars) masses, respectively, in the high-resolution simulation box. The results are in the last column of Table 1, These efficiencies are higher by a factor of roughly four than the observed values, recently measured by Guo et al. (2010a) to be $\sim 20\%$ (or $\sim 4\%$ as a fraction of total mass rather than baryons) for halos of mass $\sim 6 \times 10^{11} M_{\odot}$, and less for other halo masses. Similar results were derived by Moster et al. (2010) (who found that efficiency is linear in mass at low masses) and Trujillo-Gomez (2010).

Figure 2 shows the baryon-conversion efficiency as a function of halo mass, using a different definition:

$$\epsilon_{*,\text{eff}} \equiv \frac{M_{*,c}}{M_{b,\text{implied}}} = \frac{\Omega_M M_{*,c}}{\Omega_b M_{\text{Halo}}} = 5 \frac{M_{*,c}}{M_{\text{Halo}}}, \quad (9)$$

where $M_{*,c}$ is the stellar mass within 0.1 virial radii of the halo center, similar to Sales et al. (2010), and the “implied” baryonic mass $M_{b,\text{implied}} \equiv M_{\text{Halo}}(\Omega_b/\Omega_M)$ is simply the mass of baryons associated with the halo well before reionization. Figure 2 is analogous to Figure 5 of Guo et al. (2010a), although the results are not directly comparable (see below). There is a factor of 1.5 – 5 reduction in star formation with the addition of the ionizing backgrounds, and that the effect is stronger in lower mass halos. However our results are still too high compared to the SDSS results by a factor of ~ 2 in the highest-mass bin, and more in the lower ones. We ascribe this discrepancy first to fact that we are not looking at any field galaxies, but only galaxies in a region specifically selected to have an overdensity and a massive central galaxy. This is clearly indicated in the figure, since SF efficiency actually increases with decreasing halo mass from $10^{11.5} M_{\odot}$ to $10^{10} M_{\odot}$: a satellite galaxy will naturally have a smaller virial radius than a field galaxy, and hence a smaller DM mass will be found by the halo finder, not to mention the enhanced star formation from the denser environment (Okamoto et al. 2008). The lack of SN-driven winds in our simulations, which would otherwise eject gas from low-mass galaxies, also makes a significant contribution; the relation between mass-loss in winds and the SFR has been verified observationally (Rupke, Veilleux & Sanders 2005) and theoretically (Oppenheimer & Davé 2005). We also note that the other recent simulations shown in Figure 2—Okamoto et al. (2005), Governato et al. (2007), Scannapieco et al. (2009),

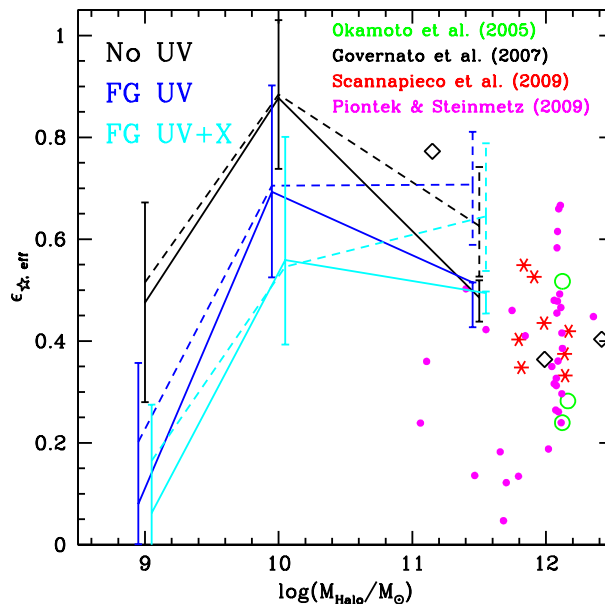


Figure 2. The baryon-conversion efficiency as function of (total, viral) halo mass. The scatter points are previous simulations. Our results, the connected error bars, are the median baryon-conversion efficiencies for 1 decade wide bins in halo mass across all 7 ICs; the error bars are the inter-quartile ranges, and there is a small horizontal offset for clarity. The solid lines are the models with SN feedback and the dashed lines are the models without it (which use 3 ICs rather than 7). The addition of the ionizing backgrounds reduces star formation by a factor of $\lesssim 5$, depending on the mass bin.

and Piontek & Steinmetz (2009)—seem to have too much star formation by factors of a few as well, and furthermore we are primarily interested in the relative differences between the various background models: thus an overall excess of star formation can be safely disregarded. As with α and fM_{crit} , there is no significant difference between the three UV-only models, or between the two UV plus X-ray models.

To explore the effect of the SN feedback on our results, we ran three sets of simulations (the A, C, and E ICs) using the No UV, FG UV and FG UV+X backgrounds with no feedback. The primary results are given in the last three rows of Table 1. The Schechter α values are somewhat steeper in each case compared to the runs with feedback, which we expect since feedback gives a direct energy injection at the site of star formation, but the differential effect of the background is much the same, although not quite as strong. In particular, the FG UV+X-F model produces an α within the observed range, showing that SN feedback, while certainly present and important, is not necessary to produce the correct spectrum of low-mass galaxies. A similar result is obtained for fM_{crit} , which increases by roughly 0.2 dex from no UV to FG UV and changes negligibly when X-rays are added. It therefore appears that the effects of the ionizing background and of SN feedback amplify one another in a superlinear fashion, as suggested by Pawlik & Schaye (2008) and Sawala et al. (2010). This is also indicated by Figure 2, where the dashed lines correspond to the no-feedback models: in the lowest-mass bin, adding feedback causes a greater

relative reduction in baryon-conversion efficiency when an ionizing background is present.

To make a detailed comparison with Sawala et al. (2010), we calculate the baryon-conversion efficiencies for a 0.2-dex-wide bin around their fiducial halo mass of $7 \times 10^8 M_\odot$. For their runs with UV background only, SN feedback only, and both, Sawala et al. (2010) give efficiencies of 0.77, 0.05, and 0.03, respectively. Here, however, the respective models FG UV-F, No UV and FG UV give median values of, respectively, 0.16, 0.47, and 0.04. So for Sawala et al. (2010), the feedback is by far the most important contributor, whereas here the background is somewhat more important. The stronger effect of the background in this work seems likely to be the effect of timing: Sawala et al. (2010) turn their background on at $z = 6$, by which time their galaxy has already created 20–30% of its final stellar mass; in our simulations, however, galaxies of this final size have no significant star formation until $z \sim 3$ (see the next subsection). Therefore our galaxies show no significant change in baryon conversion between Old UV, which turns on at $z = 6$, and FG UV, which turns on at $z = 10$, but we speculate that if the Sawala et al. (2010) runs were to be repeated with FG UV, the background would have a more significant effect. The relatively weak effect of feedback for our models, on the other hand, is likely the effect of environment: the relatively dense environment and corresponding IGM pressure on our small halos means that they do not have enough supernova energy to unbind their gas.

The physical mechanisms governing the interaction between feedback and the background radiation are beyond the scope of this paper, but our results are consistent with a picture where feedback moves gas from the centers of halos to the outer regions, where the background then provides enough energy to unbind the gas altogether. Thus there is no change in the fM_{crit} when X-rays are added in the absence of feedback because the dense central gas has too short a cooling time to be affected (although the smallest halos with the lowest central densities can still be suppressed, increasing α), whereas if it were first pushed out somewhat by feedback the density would be lower, the cooling time longer and X-rays could have an effect. Conversely, with feedback and no background (the No UV case), the gas gets pushed outward, but not enough to unbind, so it falls back in and forms more stars.

4.2 Evolution with Time

To investigate the origins of the discrepancies in low-mass systems, we examine the simulations at higher redshifts. Figure 3 shows the stellar mass spectrum of the FG UV simulations from $z = 4$ to the present. The number of low-mass systems peaks at $z \approx 2 - 3$ and then declines as small systems merge into larger ones. This peak is somewhat later than the overall star-formation peak, found in Paper I to be at $z \approx 4$, which is precisely the “downsizing” effect first reported by Cowie et al. (1996) (see Zheng et al. 2007, for more recent observational results). This effect explains why our three UV models show such similar results here: at $z = 4$ the Old UV and FG UV models have not finished HeII reionization, and Old UV has ~ 3 times lower ionization rate than the other two models, while for $z \leq 3$ the three models are nearly identical in ionization rate and have all fully reion-

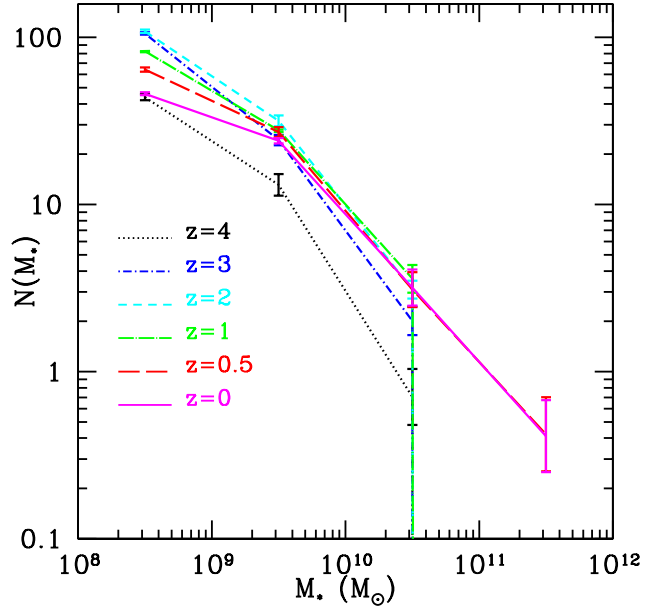


Figure 3. The mass spectrum (average number of systems per decade of mass) of stellar systems with the FG UV background at various epochs. The number of small galaxies peaks at $2 \lesssim z \lesssim 3$.

ized (see Figure 1 of Paper I). Thus at the epoch when the smallest halos are forming stars, the gas temperatures in the three models are much more similar than when stars in more dense regions formed (gas temperatures are plotted in Figure 2 of Paper I). On the other hand, the models with X-rays have higher gas temperatures than the UV-only models for all $z < 4$, which is reflected in the increased suppression of small systems.

Table 2 compares the total number of identified (stellar) systems in the whole box for the No UV and FG UV cases, as well as the baryon conversion efficiency $\epsilon_{*,\text{eff}}$, defined in Equation 9, for two bins in halo mass ($10^{8.5} < (M_{\text{Halo}}/M_\odot) < 10^{9.5}$ and $10^{10.5} < (M_{\text{Halo}}/M_\odot)$). Although No UV has ~ 3 times the number of systems as FG UV, they both show the same time dependence: the number of systems reaches a peak at $2 \lesssim z \lesssim 3$, followed by mergers reducing the number. The stellar mass fraction for high-mass halos is nearly the same for the two models, while for low-mass halos the difference is a factor of 2–6. Interestingly, in the FGUV case the low-mass stellar mass fraction declines somewhat from $z = 2$ to 0, presumably because closer satellites of the central galaxy, which had been able to form more stars than the average because of their denser environment, are finally accreted and lost (while with No UV all satellites can form many stars).

Next, we test the validity of our physical argument by comparing the mean gas temperature of the simulations at $z = 3$ (when the small systems are forming) to their critical cutoff masses at $z = 0$. (In calculating the mean gas temperature we do not separate dense galactic gas from the IGM; however at $z = 3$ only $\sim 5\%$ of gas is at virial densities, so any contamination is less than the variance of our ICs.) Our theory predicts $M_{\text{crit}} \propto T^{1.5}$. Figure 4 shows the data from our six background models together with the best-fit power law. We find that $M_{\text{crit}} \propto T^{1.54 \pm 0.17}$, in good agree-

Table 2. Stellar system statistics over time

z	$\epsilon_{*,\text{eff}}$				N	
	low-mass		high-mass		No UV	FG UV
4	.111	.052	.546	.569	153	63
3	.266	.140	.610	.618	425	159
2.5	.325	.180	.640	.650	503	174
2	.400	.220	.646	.637	567	169
1	.467	.165	.728	.730	526	134
0.5	.475	.118	.739	.792	449	109
0.0	.475	.080	.787	.776	328	82
2.5	.173	.353	.697	.712	259	443
0.5	—	.010	—	.804	—	166

The baryon conversion efficiency for low-mass ($10^{8.5} < (M_{\text{Halo}}/M_{\odot}) < 10^{9.5}$) and high-mass ($10^{10.5} < (M_{\text{Halo}}/M_{\odot})$) halos, and total number of stellar systems, for the No UV and FG UV backgrounds at various epochs. Statistical errors are $\sim 20\%$ for the first six rows. The last two rows, below the line, are the 200^3 simulations of halo A.

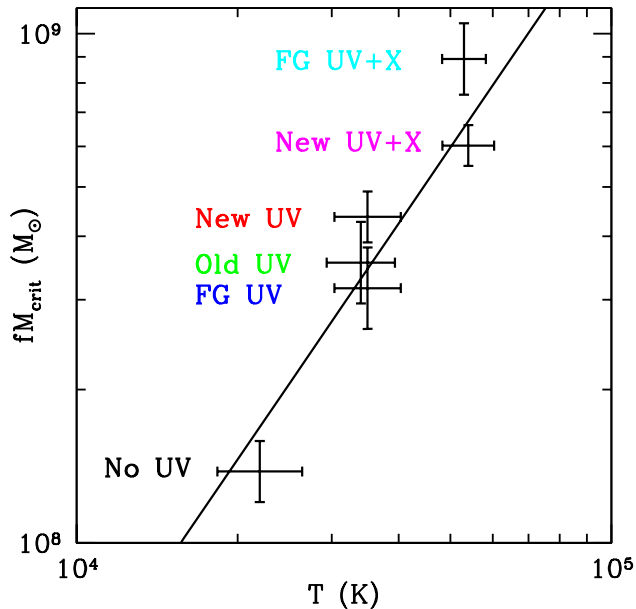


Figure 4. The critical star-free halo mass at $z = 0$ versus the mean gas temperature at $z = 3$ for each background model, together with the best-fit power law. Vertical and horizontal error bars represent 1σ statistical errors among the 7 ICs. We find $\log M_{\text{crit}} \propto (1.54 \pm 0.17) \log T$, in good agreement with the theoretical value of 1.5.

ment with the theoretical value. The goodness-of-fit statistic $\chi^2/\text{d.f.} = 1.8$ for this fit. Notice that even in the No UV case stellar feedback and dynamical heating are sufficient for the gas to reach 2×10^4 K by $z = 3$ (the gas has reionized by this epoch), but the UV heating increases the temperature by a factor of 1.6, and the X-rays by another factor of 1.5.

Finally, we examine the level of numerical convergence in our results. We perform simulations of galaxy A with 200^3 SPH particles (i.e. twice the spatial resolution and

eight times the mass resolution) with the No UV and FG UV backgrounds (and including feedback). Due to computational constraints, the No UV simulation was run only to $z = 2.5$, and the FG UV to $z = 0.5$. At $z = 2.5$, the Schechter α values for No UV and FG UV with 200^3 resolution are -1.39 and -1.33 , respectively. These values are more similar than the 100^3 runs, which have $\alpha = -1.45$ for No UV and $\alpha = -1.07$ for FG UV at the same redshift. The steepening slope for FG UV as resolution increases is explained by smaller stellar systems which are allowed by the higher peak densities associated with increased mass resolution, and which merge away at late times to flatten the low-mass slope once again (whereas No UV can keep making new small systems). Indeed, at $z = 0.5$, FG UV 200^3 has $\alpha = -1.10$, compared to the 100^3 run $\alpha = -0.95$ (and No UV 100^3 $\alpha = -1.57$). Meanwhile, the No UV 200^3 simulation at $z = 2.5$ still has a large number of small stellar systems which have not yet formed stars, and whose gas is disrupted by the background in the FG UV run. In fact, 65% of the identified halos in No UV 200^3 at $z = 2.5$ are in this category, compared to only 39% for the 100^3 case. However, the overall baryon-conversion efficiency is not significantly different as a function of resolution, at either $z = 2.5$ ($< 8\%$ difference) or $z = 0.5$ (3%). The last two rows of Table 2 show the breakdown by mass. FG UV 200^3 has a much lower efficiency than 100^3 in the low mass bin at $z = 0.5$. This is the result of the same mechanism just discussed: the increased resolution allows small halos to form and merge while remaining star-free because of the UV background. Further, at $z = 2.5$ FG UV 200^3 has a higher efficiency than No UV 200^3 . This is again the effect of proximity: while No UV has twice the number of halos in the low-mass bin as FG UV, FG UV's are preferentially close to the central galaxy and thus have lower virial masses and more efficient star formation, and increased numerical resolution allows them to exist even closer without being lost to the halo finder. (At the 25th percentile of galaxies, FG UV has roughly a tenth the efficiency of No UV in this mass bin at both resolutions.) Finally, the fM_{crit} statistic is not strongly affected by the increase in resolution: at $z = 2.5$, $\log fM_{\text{crit}} = (8.54, 8.76)$ for (No UV, FG UV), compared to $(8.47, 8.85)$ for the respective 100^3 runs. Thus we assert that our results at $z = 0$ would not be qualitatively different with increased resolution, and quantitatively different by at most 15%.

5 DISCUSSION & CONCLUSIONS

In Paper I, we examined the detailed effects on galaxy properties of modest changes to the ionizing radiation background (specifically the intensity at high z). Here we have simulated seven different galaxies with their satellites, using six different models of the ionizing background, and found that any UV background is sufficient to replicate the observational results of the low end of the galaxy mass spectrum, as parametrized by Schechter α . The details of the spectrum and redshift dependence of the background seem to have no significant effect. We find that the number of small ($< 10^9 M_{\odot}$ in stars) systems at $z = 0$ correlates with the critical star-free halo mass, which in turn correlates well with the mean gas temperature at $z = 3$. Further, the value of

our critical mass agrees with other recent studies of small galaxies. These simulation results are consistent with our theoretical picture, where only halos with an escape velocity greater than the sound speed of the gas can retain their gas long enough for it to cool and form stars.

Thus we find the addition of an X-ray background causes additional suppression of low-mass halos (by further increasing the mean temperature of the gas), making the low-mass spectrum too flat compared with observations. It is possible that this is the result of optical depth/self-shielding effects not being included in the code, thus making the UV background more efficient at heating/ionization than it is in reality. Optical depth in general decreases with harder radiation, so the optically-thin assumption is valid for X-rays. However, the small halos which we study here have the lowest densities and thus are the least effective self-shielders: Sawala et al. (2010) found that systems below the threshold mass of $10^9 M_\odot$ had their gas densities sufficiently reduced by feedback and that self-shielding of the UV background was not important. Our resolution study weakly indicates that α may decrease with increasing resolution, and a future paper (Hambrick et al., 2010, in prep.) finds that including AGN thermal feedback causes α to decrease modestly as well, presumably by driving gas back out of the central galaxy to form stars in satellites. This is certainly an area deserving further study.

We also study the baryon-conversion efficiencies of small halos, and find that for small halos in the neighborhood of massive ones, and find that the background is at least equally important as SN feedback for lowering the efficiency to observed values, in contrast to isolated dwarfs where feedback is the dominant mechanism.

In sum, reproducing the observed numbers of low-mass galaxies in hydrodynamic simulations is no problem at all, being adequately resolved by the heating mechanisms already included in standard hydro codes: feedback and the ionizing background.

JPO was supported by NSF grant AST 07-07505 and NASA grant NNX08AH31G. DCH thanks Ludwig Oser for invaluable debugging assistance. TN and PHJ acknowledge support by the DFG cluster of excellence ‘Origin and Structure of the Universe’.

REFERENCES

- Alimi, J.-M. & Courty, S., 2005, *A&A*, 433, 17
 Belokurov, V. et al., 2007, *ApJ*, 654, 897
 Belokurov, V. et al., 2006, *ApJ*, 647, 111
 Benson, A.J., Cole, S., Frenk, C.S., Baugh, C.M., Lacey, C.G., 2000, *MNRAS*, 311, 793
 Benson, A. J., Lacey, C. G., Baugh, C. M., Cole, S., Frenk, C. S., 2002, *MNRAS*, 333, 156
 Blanton, M.R., et al., 2001, *ApJ*, 121, 2358
 Chiu, W., Gnedin, N.Y., & Ostriker, J.P., 2001, *ApJ*, 563, 21
 Cooray, A., & Sheth, R., 2002, *Phys. Rep.*, 372, 1
 Cowie, L.L., Songaila, A., Hu, E.M., Cohen, J. G., 1996, *AJ*, 112, 839
 Crain, R.A., et al., 2007, *MNRAS*, 377, 41
 Crain, R.A., et al., 2009, *MNRAS*, 399, 1773
 Dekel, A., & Silk, J., 1986, *ApJ*, 303, 39
 De Lucia G., Blaizot J., 2007, *MNRAS*, 375, 2
 Efstathiou, G., 1992, *MNRAS*, 256, 43
 Faucher-Giguère, C.-A., Lidz, A., Zaldarriaga, M., Hernquist, L., 2009, arXiv:0901.4554
 Ferland, G. J., Korista, K.T., Verner, D.A., Ferguson, J.W., Kingdon, J.B., & Verner, E.M., 1998, *PASP*, 110, 761
 Gilli, R., Comastri, A., Hasinger, G., 2007, *A&A*, 463, 79
 Gnedin, N. Y., 2000, *ApJ*, 542, 535
 Governato, F., Willman, B., et al., 2007, *MNRAS*, 374, 1479
 Guo, Q., White, S., Li, C., & Boylan-Kolchin, M., 2010a, *MNRAS*, 404, 1111
 Guo, Q., et al., 2010b, arXiv:1006.0106
 Haardt, M. & Madau, P., 1996, *ApJ*, 461, 20
 Hambrick, D.C., Ostriker, J.P., Naab, T., & Johansson, P.H., 2009, *ApJ*, 705, 1566
 Hoeft, M., Yepes, G., Gottlöber, S., & Springel, V., 2006, *MNRAS*, 371, 401
 Hopkins, P.F., Richards, G.T., & Hernquist, L., 2007, *ApJ*, 654, 731
 Johansson, P.H., Naab, T., & Ostriker, J.P., 2009, *ApJ*, 697, 38
 Kay, S.T., Pearce, F.R., Frenk, C.S., Jenkins, A., 2002, *MNRAS*, 330, 113
 Kelly, B.C., Fan, X., & Vestergaard, M., 2008, *ApJ*, 682, 874
 Klypin, A., Kravtsov, A.V., Valenzuela, O., & Prada, F., 1999, *ApJ*, 522, 82
 Knollmann, S.R. & Knebe, A., 2009, *ApJS*, 182, 608
 Kravtsov, A.V., Gnedin, O.Y., & Klypin, A.A., 2004, *ApJ*, 609, 482
 Madau, P. & Efstathiou, G., 1999, *ApJ*, 517, 9
 McCarthy, I.G., et al., arXiv:0911.2641
 Moster, B.P., Somerville, R.S., Maulbetsch, C., van den Bosch, F.C., Macciò, A.V., Naab, T., Oser, L., 2010, *ApJ*, 710, 903
 Naab, T., Johansson, P.H., Ostriker, J.P., & Efstathiou, G. 2007, *ApJ*, 658, 710
 Nagamine, K., Cen, R., Hernquist, L., Ostriker, J.P., Springel, V., 2005, *ApJ*, 618, 23
 Navarro, J.F., & Steinmetz, M., 1997, *ApJ*, 478, 13
 Okamoto, T., Eke, V.R., Frenk, C.S., & Jenkins, A., 2005, *MNRAS*, 363, 1299
 Okamoto, T. & Frenk, C.S., 2009, arXiv:0909.0262
 Okamoto, T., Gao, L., & Theuns, T., 2008, *MNRAS*, 390, 920
 Oppenheimer, B.D. & Davé, R., 2006, *MNRAS*, 373, 1265
 Oppenheimer, B.D., et al., arXiv:0912.0519
 Pawlik, A.H., Schaye, J., 2008, arXiv:0812.2913
 Pérez-González, P.G., et al., 2008, *ApJ*, 675, 234
 Petkova, M., & Springel, V., 2010, arXiv:1008.4459
 Piontek F., & Steinmetz M., 2009, arXiv:0909.4167
 Press, W.H., & Schechter, P., 1974, *ApJ*, 187, 425
 Quinn, T., Katz, N., Efstathiou, G., 1996, *MNRAS*, 278, 49
 Rees, M.J., 1986, *MNRAS*, 218, 25
 Ricotti, M., Gnedin, N.Y., Shull, J.M., 2008, *ApJ*, 685, 21
 Rupke, D.S., Veilleux, S., & Sanders, D.B., 2005, *ApJS*, 160, 115
 Sales, L.V., Navarro, J.F., Schaye, J., Dalla Vecchia, C., Springel, C., & Booth, C.M., 2010, arXiv:1004.5386

- Sawala, T., Scannapieco, C., Maio, U., & White, S., 2010, MNRAS, 402, 1599
- Sazonov, S.Yu., Ostriker, J.P., & Sunyaev, R.A. 2004 MNRAS, 347, 144
- Scannapieco, C., White, S.D.M., Springel, V., Tissera, P.B., 2009, MNRAS, 396, 696
- Scannapieco, C., Tissera, P.B., White, S.D.M., & Springel, V., 2008, MNRAS, 389, 1137
- Schechter, P., 1976, ApJ, 203, 297
- Simon, J.D. & Geha, M., 2007, ApJ, 670, 313
- Somerville, R.S., 2002, ApJ, 572, 23
- Springel, V. & Hernquist, L. 2003, MNRAS, 339, 289
- Springel, V., et al., 2005, Nature, 435, 629
- Shaviv, N.J. & Dekel, A., 2003, astro-ph/0305527
- Thoul, A. A. & Weinberg, D.H., 1996, ApJ, 465, 608
- Trujillo-Gomez, S., Klypin, A., Primack, J., Romanowsky, A.J., 2010, arXiv:1005.1289
- Willman, B. et al., 2005, ApJ, 626, 85
- Yepes, G., Kates, R., Khokhlov, A., Klypin, A., 1997, MNRAS, 284, 235
- Zheng, X.Z., Bell, E.F., Papovich, C., Wolf, C., Meisenheimer, K., Rix, H.-W., Rieke, G.H., & Somerville, R., 2007, ApJ, 661, 41